Reactions of Laser-Ablated Mo and W Atoms, Cations, and Electrons with CO in Excess Neon: Infrared Spectra and Density Functional Calculations on Neutral and Charged Unsaturated Metal Carbonyls

Lester Andrews,* Mingfei Zhou,† and Gennady L. Gutsev

Chemistry Department, P. O. Box 400319, University of Virginia, Charlottesville, Virginia 22904-4319

Received: September 12, 2002; In Final Form: December 4, 2002

Laser-ablated Mo and W atoms react with CO in excess neon to give the same unsaturated $M(CO)_{3,4,5}$ carbonyls observed from photodissociation of $M(CO)_6$. The observed neon matrix fundamentals for these $M(CO)_{3,4,5}$ species bridge previous argon matrix and gas phase values. The $M(CO)_2$ dicarbonyls absorb at 1895.2 and 1884.5 cm^{-1}, and the MCO monocarbonyls absorb at 1881.2 and 1859.9 cm^{-1} for Mo and W, respectively. The $M(CO)_{1,2}^+$ cations and $M(CO)_{1,2}^-$ anions are observed as the ablation process also provides cations and electrons. Density functional theory calculations support the product identifications and vibrational assignments.

Introduction

Unsaturated transition metal carbonyls are important in catalytic reactions and organometallic synthesis.[1−3] Group 6 carbonyl intermediates were investigated first because of the availability of hexacarbonyl precursor molecules. Chromium carbonyl intermediates were examined first in rare gas matrices[4−10] and the gas phase.[11−13] Turner et al. characterized $M(CO)_n$ ($n = 3-5$) by matrix infrared spectroscopy and determined C_{3v}, C_{2v}, and C_{4v} structures, respectively, for these intermediates.[6−9] This early work has been reviewed recently.[14] Time-resolved gas phase infrared spectra provide evidence that the unsaturated group 6 carbonyls adopt the same structures in the gas phase.[11−13,15,16]

The CrCO molecule was first characterized by Weltner et al. with a 1977 cm^{-1} absorption prepared from thermal Cr atoms and CO diluted in argon.[10] Laser-ablated Cr and CO gave a 1975.6 cm^{-1} argon matrix absorption and a strong 2018.4 cm^{-1} band for CrCO in solid neon,[17] which is a relatively large argon-to-neon matrix shift.[18] The CrCO molecule was predicted to have a bent high-spin $^7A'$ ground state, which correlates with ground state Cr atom (^7S) and CO ($^1\Sigma^+$).[19−21] In contrast, the MoCO and WCO complexes were computed to have low-spin ground states,[22] which arise from the smaller Mo and W exchange terms than found for Cr. Because the low-spin state has lower repulsion due to s to d promotion and more metal to CO π donation, the C−O stretching frequencies decrease significantly to 1862.6 and 1848.8 cm^{-1}, respectively, for MoCO and WCO in solid argon.[23]

We report here a combined neon matrix infrared experimental and density functional theoretical investigation of the unsaturated Mo and W carbonyls with emphasis on the smaller coordination numbers and the new neon matrix observations for charged species. In these laser ablation experiments, metal cations and electrons are also produced and several charged metal carbonyl species are also trapped.

* To whom correspondence should be addressed. E-mail: lsa@virginia.edu.
† Present address: Department of Chemistry, Fudan University, Shanghai 200433, P. R. China.

Experimental and Computational Methods

The experimental method for laser ablation and matrix isolation has been described in detail previously.[24−26] Briefly, the Nd:YAG laser fundamental (1064 nm, 10 Hz repetition rate with 10 ns pulse width) was focused to irradiate rotating metal targets (Johnson−Matthey). Typically, low laser power (3−5 mJ/pulse) was used, which favors the stabilization of ionic species and minimizes cluster formation. Laser-ablated metal atoms, cations, and electrons were codeposited with carbon monoxide (0.1−0.4%) in excess neon onto a 4−5 K CsI cryogenic window at 2−4 mmol/h for 30 min. Carbon monoxide (Matheson) and isotopic $^{13}C^{16}O$ and $^{12}C^{18}O$ (Cambridge Isotopic Laboratories) and selected mixtures were used in different experiments. Infrared spectra were recorded at 0.5 cm^{-1} resolution on a Nicolet 750 spectrometer with 0.1 cm^{-1} accuracy using a mercury cadmium telluride detector down to 400 cm^{-1}. Matrix samples were annealed at different temperatures, and selected samples were subjected to photolysis using a medium-pressure mercury lamp ($\lambda > 240$ nm) with the globe removed.

Density functional theory (DFT) calculations were performed on the small reaction products using the GAUSSIAN 98 program.[27] Two generalized gradient approximations consisting of the combinations of Becke's exchange and Perdew's correlation (BP86) and Becke's exchange and Perdew−Wang's correlation (BPW91) functionals[28] as well as the hybrid Hartree−Fock B3LYP functional[29] were chosen in order to reinforce each other. The 6-31+G* and 6-311+G* basis sets were used for carbon and oxygen[30] and the LanL2DZ effective core potentials were used for Mo and W.[31,32]

Results and Discussion

Neon matrix infrared spectra illustrated in Figures 1−7 will be assigned to Mo and W carbonyls and compared to previous observations and DFT frequency calculations.

MCO. As part of an investigation of the group 6 metal atom reaction with CO_2, dilute CO was reacted with these metals in excess argon, and CrCO, MoCO, and WCO were the major products. Isotopic mixtures were employed to confirm the participation of a single CO subunit. The C−O fundamentals were 1975.3, 1862.6, and 1848.8 cm^{-1}, respectively, for the group 6 monocarbonyls.[23]

10.1021/jp026978v CCC: $25.00
Published on Web 01/24/2003

TABLE 1: Infrared Absorptions (cm^{-1}) from Reactions of Laser-Ablated Mo with CO in Excess Neon

$^{12}C^{16}O$	$^{13}C^{16}O$	$^{12}C^{18}O$	R(12/13)	R(16/18)	assignment
3899.5	3813.3	3809.7	1.0226	1.0236	$Mo(CO)_2$, $a_1 + b_2$
3730.7	3645.0	3650.3	1.0235	1.0220	MoCO, 2ν(CO)
2194.3	2145.8		1.0226		CO^+
2189.1		2137.3		1.0242	$MoCO^+$
2187.7		2135.9		1.0243	$MoCO^+$ site
2178.2	2129.6	2127.1	1.0228	1.0240	$Mo(CO)_2^+$
2140.8	2093.7	2098.7	1.0225	1.0245	CO
2056.3	2010.9	2007.4	1.0226	1.0224	$(CO)_2^+$
2000.6	1956.6	1952.8	1.0225	1.0245	$Mo(CO)_6$
1984.5	1941.2	1936.6	1.0223	1.0247	$Mo(CO)_5$, e
1965.7	1922.7	1918.3	1.0224	1.0247	$Mo(CO)_4$, b_2
1944.6	1900.1	1901.1	1.0234	1.0229	$Mo(CO)_5$, a_1
1938.2	1896.2	1891.1	1.0221	1.0249	$Mo_x(CO)_y$
1914.3	1872.7	1868.5	1.0222	1.0245	$Mo_x(CO)_y$
1908.9	1865.6	1866.0	1.0232	1.0230	$Mo(CO)_4$, b_1
1895.2	1854.6	1848.9	1.0219	1.0250	$Mo(CO)_2$, b_2
1886.1	1842.9	1843.8	1.0234	1.0229	$Mo(CO)_3$, e
1881.2	1837.5	1840.2	1.0238	1.0223	MoCO, ν(CO)
1878.3	1834.7	1837.4	1.0238	1.0223	MoCO site
1797.7	1758.5	1755.3	1.0223	1.0242	$Mo_2(CO)_2$
1771.4	1729.2	1735.2	1.0244	1.0209	$(Mo(CO)_3^-)$
1718.7	1680.6	1678.7	1.0227	1.0238	$Mo(CO)_2^-$
1699.6	1659.3	1663.9	1.0243	1.0215	$(MoCO)^-$
1517.4	1484.2	1481.2	1.0224	1.0244	$(CO)_2^-$
598.6	585	595	1.023	1.006	$Mo(CO)_6$

TABLE 2: Infrared Absorptions (cm^{-1}) from Reactions of Laser-Ablated W with CO in Excess Neon

$^{12}C^{16}O$	$^{13}C^{16}O$	$^{12}C^{18}O$	R(12/13)	R(16/18)	assignment
3687.0	3607.6	3605.8	1.0220	1.0225	WCO, 2ν(CO)
2194.3	2145.8		1.0226		CO^+
2125.5	2077.8	2076.5	1.0230	1.0236	WCO^+
2122.4	2074.6	2073.6	1.0230	1.0235	WCO^+ site
2056.3	2010.9	2007.4	1.0226	1.0224	$(CO)_2^+$
1995.3	1951.0	1948.1	1.0227	1.0242	$W(CO)_6$
1975.9	1932.3	1929.0	1.0226	1.0243	$W(CO)_5$, e
1954.0	1910.9	1907.2	1.0226	1.0245	$W(CO)_4$, b_2
1941.1	1896.2	1898.4	1.0237	1.0225	$W(CO)_5$, a_1
1909.0	1864.7	1867.2	1.0238	1.0224	$W(CO)_4$, b_1
1903.7	1860.2	1861.8	1.0234	1.0225	$W_x(CO)_y$
1884.5	1843.4	1839.3	1.0223	1.0246	$W(CO)_2$, b_2
1882.4	1838.3	1841.2	1.0240	1.0224	$W(CO)_3$, e
1859.9	1818.8	1818.0	1.0226	1.0230	WCO, ν(CO)
1821.8	1779.9	1781.9	1.0235	1.0224	$W_2(CO)_2$
1794.2	1751.8	1755.2	1.0242	1.0222	$W(CO)_3^-$, e
1751.5	1712.2	1711.0	1.0230	1.0237	$W(CO)_2^-$, b_2
1640.8	1603.3	1606.5	1.0234	1.0214	WCO^-
1706.2	1666.5				weak
1517.4	1484.2	1481.2	1.0224	1.0244	$(CO)_2^-$
588.5		584.9		1.0062	$W(CO)_6$

The present neon matrix investigations produced strong absorptions at 1881.2 and 1859.9 cm^{-1} that increased on annealing (Figures 1 and 5) and showed appropriate isotopic shifts and the doublet mixed $^{12}CO + {}^{13}CO$ isotopic behavior for assignment to the monocarbonyls MoCO and WCO (Figures 4 and 7). Note that the argon-to-neon blue shifts, 18.6 and 11.1 cm^{-1}, are much less than found for CrCO (43.1 cm^{-1}).[17]

In contrast to CrCO, the first overtone was observed for the C−O fundamentals of both MoCO and WCO. Although the MoCO overtone is weak (1.2% of fundamental intensity) the site-splitting pattern on the fundamental made matching the overtone straightforward. For MoCO, the major site at 3736.6 cm^{-1} is 25.8 cm^{-1} below twice the fundamental (1881.2 cm^{-1}) (Table 1). The WCO overtone at 3687.0 cm^{-1} is stronger (6% of the fundamental) and 32.8 cm^{-1} below twice the fundamental (1859.9 cm^{-1}) (Table 2). Hence, the WCO mode is more anharmonic than the MoCO mode, which is in turn more anharmonic than the CrCO mode where no overtone was detected.

Tan et al.[22] have performed a high-level theoretical investigation of MoCO and WCO. At the multireference singles plus doubles configuration interaction level, the ground state of MoCO is $^5\Sigma^+$ and the CO fundamental is 2183 cm^{-1}. The slightly higher energy $^5\Phi$ and $^3\Delta$ states have slightly higher 2196 and 2202 cm^{-1} computed harmonic frequencies. On the other hand, the ground state for WCO is predicted to be $^7\Sigma^+$ with CO fundamental 2176 cm^{-1} and the slightly higher $^5\Sigma^+$ state has virtually the same (2177 cm^{-1}) frequency. When spin−orbit coupling is taken into account, the low-lying states are predominantly $^7\Sigma^+$ and the frequency is the same within ±4 cm^{-1}. These high level calculations show that the MoCO frequency is slightly higher (20 ± 10 cm^{-1}) than the WCO frequency and that spin−orbit coupling has little effect on the C−O stretching frequency.

Despite the lack of multireference character, DFT calculations have reliably predicted the C−O fundamentals of second and third row monocarbonyls.[14] Accordingly, we have performed BP86 and B3LYP calculations for MoCO and WCO to provide support for assignment of experimental frequencies. DFT predicts ground states unresolved by symmetry, which are probably $^5\Pi$ for both MoCO and WCO with the vibrational frequency for MoCO higher than for WCO by 26 (BP86) or 37 cm^{-1} (B3LYP). The neon matrix separation is 21.3 cm^{-1}. The 1876 and 1850 cm^{-1} predictions (BP86, 6-311+G*) for MoCO and WCO are 5 and 10 cm^{-1}, respectively, lower than observed values. Using BP86, the $^7A'$ states for MoCO and WCO are 13.9 kcal/mol higher, and the frequencies are 28 and 25 cm^{-1} higher than observed. These DFT calculations support our matrix infrared assignments for MoCO and WCO.

$Mo(CO)_2$. The absorption at 1895.2 cm^{-1} with Mo and CO in neon increased markedly on annealing and dominated all other absorptions: it decreased on visible photolysis but restored on further annealing (Figure 1). This band shifted to 1848.9 cm^{-1} with $C^{18}O$ and to 1854.6 cm^{-1} with ^{13}CO and formed a strong sharp 1895.2−1871.8−1854.6 cm^{-1} triplet with mixed ^{12}CO and ^{13}CO (Figure 4), which denotes the vibration of two equivalent CO subunits and the identification of $Mo(CO)_2$. The central component is 3.1 cm^{-1} below the median of pure ^{12}CO and ^{13}CO components, which points to interaction with the symmetric C−O stretching mode of $Mo(^{12}CO)(^{13}CO)$ some 100 cm^{-1} higher. Although no such fundamental was observed, its combination with the 1895.2 cm^{-1} antisymmetric stretching fundamental was found at 3899.5 cm^{-1} with identical annealing and photolysis behavior and 1% of the absorbance at 1895.2 cm^{-1}. The combination band gave a similar 1:2:1 triplet at 3899.5−3859.4−3813.3 cm^{-1} using mixed ^{12}CO and ^{13}CO (Figure 3), and the central component is 2.9 cm^{-1} above the median of 3899.5 + 3813.3 cm^{-1}. The difference 3899.5 − 1895.2 = 2004.3 cm^{-1}. Adding an estimated 25 cm^{-1} correction for anharmonicity[33] from $Ni(CO)_2$ gives a 2029 cm^{-1} prediction for the symmetric C−O fundamental in $Mo(CO)_2$.

Our assignment of 1895.2 cm^{-1} to the b_2 mode of $Mo(CO)_2$ in solid neon is in agreement with an argon matrix 1891.9 cm^{-1} observation from earlier work[23] but not with a tentative assignment of a weak 1911 cm^{-1} band (system "c") in solid methane.[8]

The analogous feature with W and CO in neon increased strongly on annealing at 1884.5 cm^{-1} and shifted to 1839.2 cm^{-1} with $C^{18}O$ and to 1843.4 cm^{-1} with ^{13}CO (Figures 5 and 6). Although $W(CO)_2$ and $W(CO)_3$ are nearly coincident for

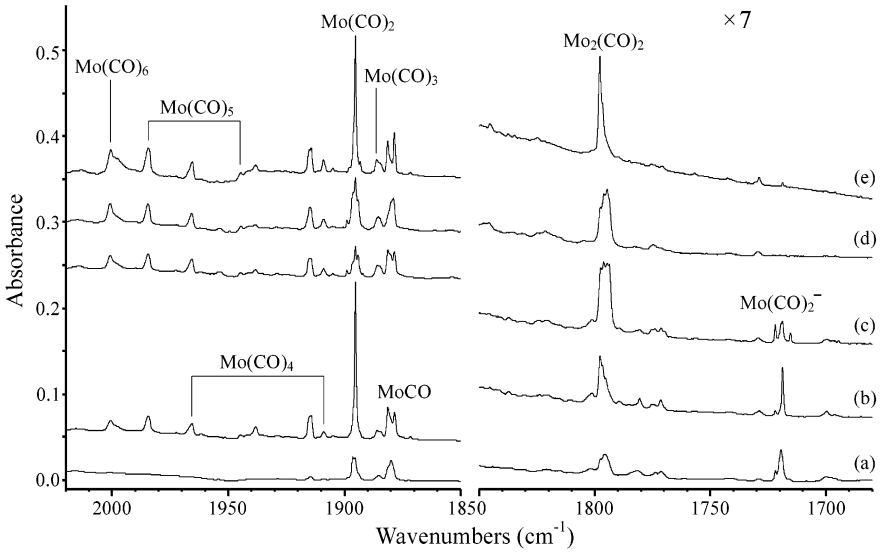

Figure 1. Infrared spectra in the 2020−1850 and 1850−1680 cm^{-1} regions for laser-ablated Mo codeposited with 0.1% CO in neon at 4 K. (a) Sample deposited for 30 min, (b) after annealing to 8 K, (c) after $\lambda > 470$ nm photolysis for 15 min, (d) after $\lambda > 290$ nm photolysis, and (e) after annealing to 10 K. Spectra in right portion multiplied by given factor to fit indicated absorbance scale.

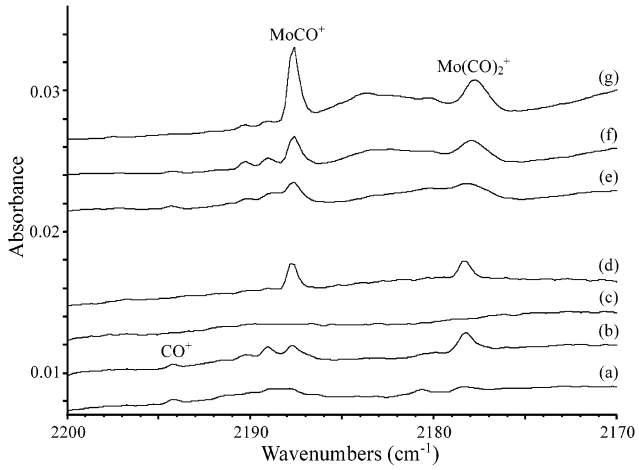

Figure 2. Infrared spectra in the 2200−2170 cm^{-1} region for laser-ablated Mo codeposited with CO in neon at 4 K. (a) Sample deposited for 30 min, (b) after annealing to 8 K, (c) after $\lambda > 240$ nm photolysis, (d) after annealing to 12 K, (e) sample with 0.02% CCl_4 added deposited for 30 min, (f) after annealing to 8 K, and (g) after annealing to 12 K.

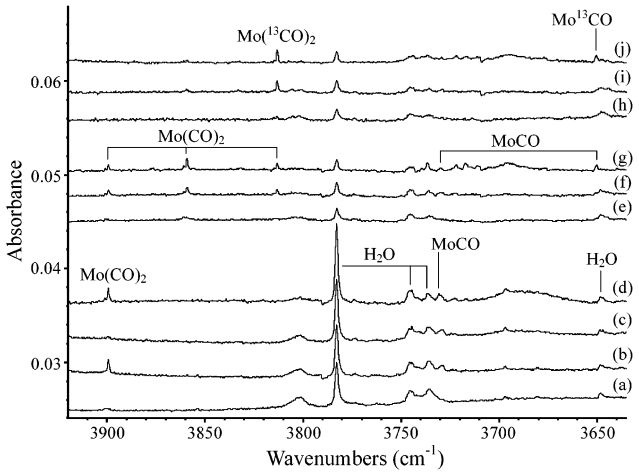

Figure 3. Infrared spectra in the 3920−3635 cm^{-1} region for laser-ablated Mo codeposited with carbon monoxide in neon at 4 K. (a) ^{12}CO (0.1%) deposited for 30 min, (b) after annealing to 8 K, (c) after $\lambda > 470$ nm photolysis for 15 min, (d) after annealing to 10 K, (e) 0.1% ^{12}CO + 0.1% ^{13}CO deposited for 30 min, (f) after annealing to 8 K, (g) after annealing to 12 K, (h) 0.2% ^{13}CO deposited for 30 min, (i) after annealing to 8 K, and (j) after annealing to 12 K.

^{12}CO, these absorptions are resolved for ^{13}CO. These bands, however, gave a broader intermediate component at 1849.9 cm^{-1} with mixed ^{12}CO + ^{13}CO (Figure 7) that does not sharpen on annealing like the pure isotopic 1884.5 and 1843.4 cm^{-1} bands. This suggests symmetry breaking for $W(CO)_2$ similar to that found for $W(NO)_4$ although $W(NO)_2$ apparently has equivalent NO subunits.[34]

Extensive DFT level calculations were performed for $Mo(CO)_2$ and $W(CO)_2$ to support the above vibrational assignments. The BP86 functional predicts $^3A_2$ ground states for both dicarbonyls, Table 5, but b_2 C−O frequencies that are 68 and 55 cm^{-1} too low and a_1 C−O frequencies that are intense enough to be observed, in contrast to experiment. However, the $^5A_2$ states, predicted some 0.6 eV higher, have b_2 modes computed 17 and 2 cm^{-1} higher than observed and weak a_1 modes, in much better agreement with experiment. Similar results were found using the B3LYP functional, as summarized in Table 6. For $Mo(CO)_2$, the $^5A_2$ state is only 0.3 eV higher than the $^3A_2$ state, probably within the energy accuracy of the calculation, and the computed frequencies are higher as expected, but the molecule is almost linear and the a_1 mode has no infrared intensity. We believe that $^5A_2$ is the ground state of $Mo(CO)_2$ observed here. It is unlikely that matrix interaction has altered the relative energy of the $^3A_2$ and $^5A_2$ states as the former has the larger dipole moment. The same rationale applies to $W(CO)_2$ although the B3LYP functional only lowers the state separation to 0.45 eV for this difficult system to model theoretically.

$M(CO)_3$. After MoCO at 1881.2 cm^{-1} and $Mo(CO)_2$ at 1895.2 cm^{-1}, annealing solid neon samples containing Mo and CO next increase 1914.3 and 1886.1 cm^{-1} bands (Figure 1). The latter is compatible with the 1862 cm^{-1} methane matrix band assigned to $Mo(CO)_3$ on the basis of the mixed isotopic quartet expected for the degenerate stretching mode of a trigonal species.[14,35] Ultraviolet ($\lambda > 240$ nm) photolysis increased the 1886.1 cm^{-1} band, which also follows the previous work. Our mixed ^{12}CO + ^{13}CO experiment is congested with $M(CO)_{1,2}$ absorptions so intermediate components for the 1886.1−1842.9 cm^{-1} bands cannot be observed. The 1886.1 cm^{-1} neon matrix

TABLE 3: Calculated (BP86) Geometries,[a] Relative Energies (kcal/mol), Vibrational Frequencies (cm^{-1}), and Infrared Intensities (km/mol) for MCO, MCO^+, and MCO^-

molecule	relative energy	geometry	$^{12}C^{16}O$	$^{13}C^{16}O$	$^{12}C^{18}O$
MoCO ($^5\Pi$)[b]	0.0	Mo−C, 1.926 Å; C−O, 1.189 Å; linear	1871.7(581), 498.9(0.1), 337.3(20)	1827.3(553), 492.8(0.1), 327.1(17)	1830.6(556), 484.6(0), 333.1(20)
MoCO ($^7A'$)	+13.9	Mo−C, 2.270 Å; C−O, 1.172 Å; 134.8°	1909.2(933), 311.0(0), 175.7(9)	1867.3(889), 300.9(9), 174.1(9)	1862.2(892), 309.3(10), 169.6(9)
$MoCO^+$ ($^6\Sigma^+$)	+165	Mo−C, 2.127 Å; C−O, 1.147 Å; linear	2119.6(256), 335.8(2), 272.8(0.7)	2071.6(241), 331.4(2), 264.8(0.7)	2069.6(249), 326.8(2), 269.2(0.6)
$MoCO^-$ ($^4\Pi$)[c]	−21.1	Mo−C, 1.911 Å; C−O, 1.202 Å linear	1759.0(1345), 504.1(15), 342.4(8)	1716.4(1270), 470.9(10), 331.0(7)	1721.1(1293), 461.9(8), 337.1(6)
$MoCO^-$ ($^4\Sigma^-$)	−26.6	Mo−C, 1.848 Å; C−O, 1.240 Å; linear	1633.2(1188), 563.6(0.3), 357.6(22)	1592.2(1134), 557.6(0.1), 346.7(20)	1601.0(1135), 546.3(0.4), 353.4(23)
WCO ($^5\Pi$)[b]	0.0	W−C, 1.905 Å; C−O, 1.195 Å; linear	1847.4(611), 522.5(2), 359.3(11)	1802.6(580), 515.6(2), 348.4(10)	1808.3(589), 505.6(1), 354.8(11)
WCO^+ ($^6\Sigma^+$)	+170	W−C, 2.017 Å; C−O, 1.152 Å; linear	2077.6(307), 425.7(9), 330.8(0.1)	2029.7(288), 419.6(9), 320.9(0.1)	2029.9(300), 412.7(8), 326.6(0.1)
WCO^- ($^4\Sigma^-$)	−25.4	W−C, 1.852 Å; C−O, 1.245 Å; linear	1623.4(1173), 561.7(2), 391.5(37)	1581.5(1119), 555.1(2), 379.5(35)	1592.9(1121), 542.1(3), 387.0(39)
WCO^- ($^4\Pi$)	−32.3	W−C, 1.904 Å; C−O, 1.210 Å; linear	1730.1(1083), 515.8(10), 328.0(2)	1687.4(1031), 509.2(0), 318.2(2)	1694.6(1038), 498.7(0), 323.8(2)
WCO^- ($^2\Delta$)	−34.4	W−C, 1.836 Å; C−O, 1.226 Å	1678.4(1409), 578.5(0), 407.2(3)	1635.3(1339), 571.7(0), 394.8(2)	1646.7(1355), 558.4(0), 402.4(3)

[a] Basis set 6-31+G* on C, O: the 6-311+G* set gave 1.928 and 1.179 Å and 1876, 495, 338 cm^{-1} for $^5\Pi$ MoCO and 1.905 Å and 1850, 522, 363 cm^{-1} for $^5\Pi$ WCO. [b] Unresolved by symmetry, probably $^5\Pi$: low frequencies are averages of split bending modes. [c] 6-311+G* basis set.

TABLE 4: Calculated (B3LYP) Geometries,[a] Relative Energies (kcal/mol), Vibrational Frequencies (cm^{-1}), and Infrared Intensities (km/mol) for the MCO, MCO^+, and MCO^-

molecule	relative energy	geometry	$^{12}C^{16}O$	$^{13}C^{16}O$	$^{12}C^{18}O$
MoCO ($^5\Pi$)[b]	0.0	Mo−C, 1.948 Å; C−O, 1.173 Å; linear	1953.3(833), 475.8(0.8), 333.9(20)	1907.7(793), 469.9(0.9), 323.9(18)	1909.3(798), 462.5(0.6), 329.7(21)
$MoCO^+$ ($^6\Sigma^+$)	+154	Mo−C, 2.127 Å; C−O, 1.147 Å; linear	2238.6(272), 285.2(3), 262.2(0.2)	2188.2(257), 281.4(2), 254.5(0.2)	2185.3(264), 277.6(2), 258.6(0.2)
$MoCO^-$ ($^4\Sigma^-$)	−19.3	Mo−C, 1.848 Å; C−O, 1.240 Å; linear	1680.9(1567), 549.5(0.5), 311.1(50)	1639.8(1493), 543.3(0.8), 302.0(46)	1646.0(1500), 533.2(0.3), 306.8(52)
WCO ($^5\Pi$)[b]	0.0	W−C, 1.916 Å; C−O, 1.180 Å; linear	1915.7(863), 509.4(5), 365.2(9)	1870.3(818), 502.5(6), 354.2(8)	1873.8(833), 493.3(5), 360.6(9)
WCO^+ ($^6\Sigma^+$)	+163	W−C, 2.044 Å; C−O, 1.137 Å; linear	2181.4(419), 400.1(14), 334.5(0)	2131.7(393), 394.2(14), 324.6(0)	2130.4(410), 388.0(13), 330.2(0)
WCO^- ($^4\Sigma^-$)	−19.1	W−C, 1.856 Å; C−O, 1.231 Å; linear	1665.0(1497), 554.1(0.1), 370.9(21)	1623.2(1426), 547.3(0.1), 359.6(79)	1632.2(1426), 535.4(0.3), 366.4(22)
WCO^- ($^4\Pi$)	−31.3	W−C, 1.909 Å; C−O, 1.205 Å; linear	1782.3(1302), 509.4(2), 355.3(0)	1739.2(1238), 502.7(2), 344.5(0)	1744.5(1250), 492.9(2), 350.9(0)

[a] Basis set 6-31+G* on C, O. [b] Unresolved by symmetry, probably $^5\Pi$; low frequencies are averages of split bending modes.

band is assigned to $Mo(CO)_3$ in line with 1862 cm^{-1} methane, 1869 cm^{-1} argon matrix,[8] and 1891 cm^{-1} gas phase values.[13]

A single intermediate component observed at 1890.3 cm^{-1} for the 1914.3−(1872.7 cm^{-1}) bands is slightly weaker but with the same profile as the 1914.3 cm^{-1} band (1872.7 cm^{-1} is masked by the very strong 1871.8 cm^{-1} $Mo(^{12}CO)(^{13}CO)$ band), and another intermediate component could also be masked. The weak 1914.3 cm^{-1} band could be due to a distorted $Mo(CO)_2$ species with two nonequivalent CO subunits, but we cannot provide more supporting evidence. This band could also be due to a higher $Mo_x(CO)_y$ species.

After WCO at 1859.9 cm^{-1} and $W(CO)_2$ at 1884.5 cm^{-1}, annealing solid neon samples containing W and CO next increases a weak 1903.7 cm^{-1} band and a shoulder absorption at 1882.4 cm^{-1}. Photolysis ($\lambda > 470$ nm) markedly reduces the 1884.5 cm^{-1} $W(CO)_2$ band and increases the 1882.4 cm^{-1}

TABLE 5: Spectroscopic Constants of $Mo(CO)_2$ and $W(CO)_2$ States Calculated at the BP86/ LANL2DZ(Mo, W)+6-311+G*(C,O) Level

	$Mo(CO)_2$				$W(CO)_2$			
	$^1A_1$	$^3A_2$[a]	$^5A_2$	$^5A_1$	$^1A_2$	$^3A_2$	$^5A_2$[b]	$^5A_1$
r_e(M−C) (Å)	1.887	1.911	2.071	2.017	1.899	1.901	2.030	1.977
r_e(C−O)	1.183	1.176	1.162	1.168	1.180	1.180	1.167	1.173
<CMC (deg)	87.7	78.1	157.6	105.6	78.0	78.7	151.3	109.7
<MCO (deg)	179.7	177.7	175.2	171.0	179.0	178.9	172.2	171.1
$\omega(a_1)$[c]	95(2)	101(1)	34(3)	72(1)	102(1)	102(1)	42(3)	76(1)
$\omega(a_2)$	377(0)	367(0)	272(0)	190(0)	391(0)	390(0)	304(0)	257(0)
$\omega(b_1)$	389(20)	391(10)	350(13)	279(1)	398(5)	399(6)	412(4)	334(0)
$\omega(b_2)$	404(7)	415(3)	270(1)	313(0)	443(3)	439(1)	302(1)	355(0)
$\omega(b_2)$	531(5)	489(22)	381(69)	397(52)	523(16)	518(22)	402(49)	431(38)
$\omega(a_1)$	533(1)	528(1)	352(4)	428(1)	545(2)	541(2)	413(1)	470(1)
$\omega(a_1)$	647(0)	622(0)	396(0)	500(1)	592(5)	595(1)	442(1)	493(0)
$\omega(b_2)$	1830(1168)	1827(1151)	1912(2432)	1880(1593)	1839(1057)	1829(1214)	1886(2312)	1860(1563)
$\omega(a_1)$	1904(436)	1936(491)	1997(60)	1938(414)	1921(616)	1927(574)	1974(107)	1919(434)
μ (Debye)	6.31	4.72	1.02	3.26	5.49	5.61	1.29	3.07
ΔE_{tot} (eV)	+0.22	0.0	+0.61	+0.87	+0.32	0.0	+0.61	+0.82
ΔE_{tot} (eV), linear	$^1\Sigma_g^+$ (+1.17)	$^3\Sigma_g^-$ (+0.90)	TS (+0.62)		$^1\Sigma_g^+$ (+0.98)	$^3\Sigma_g^-$ (+0.74)	TS (+0.63)	

[a] $^3B_1$ is by 0.19 eV above; $\omega(b_2)$ = 1784[2095], $\omega(a_1)$ = 1926[359]. [b] $^3B_1$ is by 0.17 eV above; $\omega(b_2)$ = 1794[2043], $\omega(a_1)$ = 1915[413]. [c] Frequency, cm^{-1} (infrared intensity, km/mol).

TABLE 6: Spectroscopic Constants of $Mo(CO)_2$ and $W(CO)_2$ Calculated at the B3LYP/LANL2DZ(Mo, W)+6-311+G*(C,O) Level

	$Mo(CO)_2$			$W(CO)_2$		
states	$^1A_1$	$^3A_2$	$^5A_2$	$^1A_2$[a]	$^3A_2$	$^5A_2$
r_e(M−C) (Å)	1.905	1.930	2.106	1.911	1.913	2.069
r_e(C−O)	1.165	1.160	1.146	1.164	1.164	1.149
<CMC (deg)	87.7	78.4	179.4	78.2	78.4	179.5
<MCO (deg)	179.3	177.4	179.9	178.8	178.7	180.0
$\omega(a_1)$ (cm^{-1})	93(2)	102(2)	32(3)	105(1)	105(1)	38(1)
$\omega(a_2)$	380(0)	367(0)	275(0)	400(0)	398(0)	307(0)
$\omega(b_1)$	397(19)	396(9)	538 (0)	409(3)	411(4)	408(0)
$\omega(b_2)$	408(7)	416(1)	276(0)	452 (1)	449 (0)	315(0)
$\omega(b_2)$	510(15)	459(44)	352(112)	508(30)	502 (43)	361(91)
$\omega(a_1)$	514(4)	508(2)	345(2)	534(8)	531 (2)	421(0)
$\omega(a_1)$	652(1)	631(0)	371(0)	611(8)	611(2)	566 (1)
$\omega(b_2)$	1904(1489)	1892(1508)	2000(3377)	1905(1372)	1889(1592)	1979(3387)
$\omega(a_1)$	1984(590)	2018(684)	2102(0)	1998(888)	2003(831)	2092(0)
μ (Debye)	6.26	5.69	1.02	5.49	5.67	0.00
ΔE_{tot} (eV)	+0.17	0.0	+0.30	+0.26	0.0	+0.45

[a] $^1A_1$ converged to a linear configuration +0.34 eV above $^1A_2$.

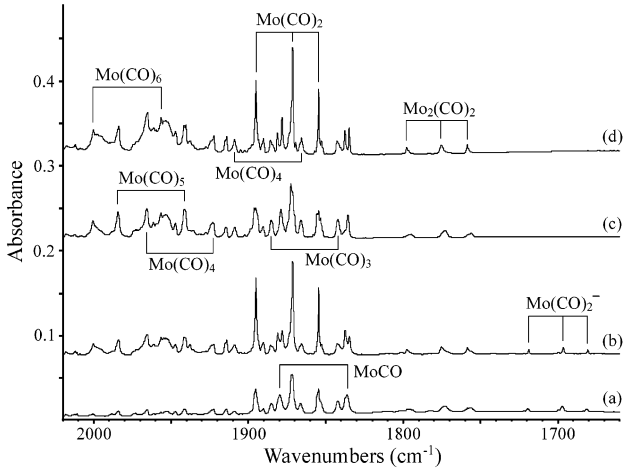

Figure 4. Infrared spectra in the 2020−1660 cm^{-1} region for laser-ablated Mo codeposited with carbon monoxide in neon at 4 K. (a) 0.1% ^{12}CO + 0.1% ^{13}CO deposited for 30 min, (b) after annealing to 8 K, (c) after λ > 240 nm photolysis for 15 min, and (d) after annealing to 10 K.

absorption (Figure 5). The $C^{18}O$ and ^{13}CO shifts to 1841.2 and 1838.3 cm^{-1}, respectively, demonstrate increased carbon and decreased oxygen participation in the normal mode relative to CO itself. Although there are band coincidences with other carbonyl species in the mixed ^{12}CO + ^{13}CO experiment, the $W(CO)_3$ absorption appears to give the characteristic quartet profile for a tricarbonyl (Figure 7). Our assignment to $W(CO)_3$ at 1882.4 cm^{-1} is in agreement with 1857 cm^{-1} methane and 1865 cm^{-1} argon matrix observations.[8]

$M(CO)_4$. Two absorptions at 1965.7 and 1908.9 cm^{-1} increase together on 6 (not shown), 8, and 10 K annealing (Figure 1). In a separate experiment with 0.2% CO, this increase is more dramatic, and full arc photolysis doubles these absorptions. Substitution of ^{13}CO and $C^{18}O$ shifts these bands appropriately for C−O vibrations (Table 1), but specific intermediate components cannot be identified in the complicated mixed isotopic experiment (Figure 4). Detailed methane matrix experiments involving photodissociation of $Mo(CO)_6$ with ^{13}-CO substitution present evidence for assigning weak 2057 and 1927 cm^{-1} absorptions to a_1 modes and strong 1945 and 1887 cm^{-1} absorptions to b_2 and b_1 modes of the C_{2v} $Mo(CO)_4$ molecule.[8] The strong bands shift to 1951 and 1895 cm^{-1} in solid argon,[8] and our 1965.7 and 1908.9 cm^{-1} neon matrix absorptions are nicely in line with the 1972 and 1911 cm^{-1} gas phase observations.[13,15]

Two absorptions at 1954.0 and 1909.0 cm^{-1} increase together on 6 (not shown) and 8 K annealing and on λ > 470 nm

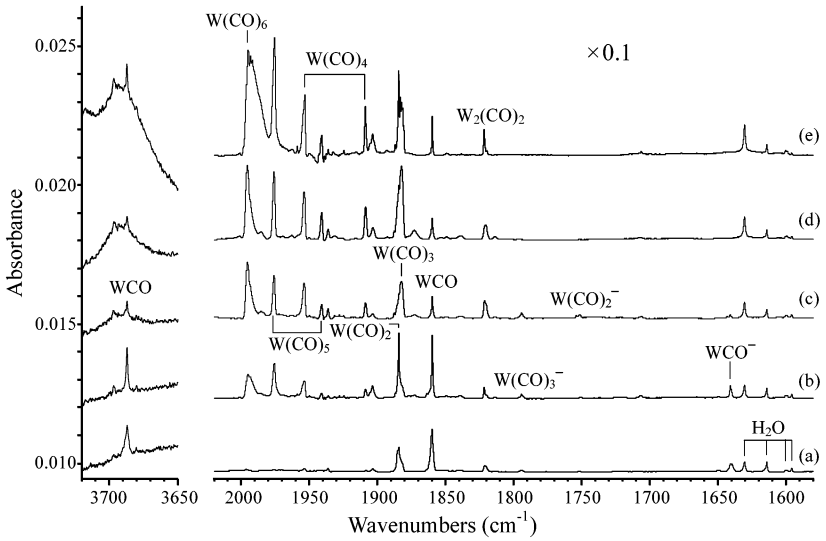

Figure 5. Infrared spectra in the 3720−3650 and 2020−1580 cm^{-1} regions for laser-ablated W codeposited with 0.1% CO in neon at 4 K. (a) Sample deposited for 30 min, (b) after annealing to 8 K, (c) after $\lambda > 470$ nm photolysis for 15 min, (d) after $\lambda > 290$ nm photolysis, and (e) after annealing to 10 K. Spectra in the right portion were multiplied by given factor to fit indicated absorbance scale.

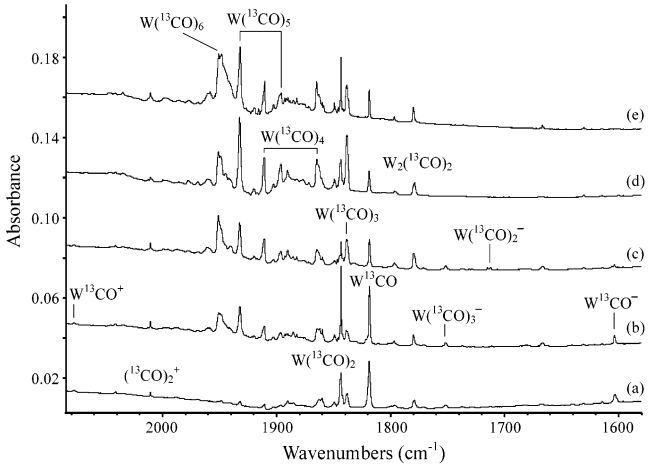

Figure 6. Infrared spectra in the 2085−1580 cm^{-1} regions for laser-ablated W codeposited with 0.2% ^{13}CO in neon at 4 K. (a) Sample deposited for 30 min, (b) after annealing to 8 K, (c) after $\lambda > 470$ nm photolysis for 15 min, (d) after $\lambda > 290$ nm photolysis, and (e) after annealing to 10 K.

photolysis with the growth of $W(CO)_3$ and demise of $W(CO)_2$ and WCO (Figure 5). This increase is, of course, more marked with 0.2% CO in another experiment. These bands exhibit appropriate ^{13}CO and C^{18}O shifts for C−O normal modes (Table 2), but the mixed isotopic experiments are too crowded to identify intermediate components (Figure 7). Again, photodissociation of $W(CO)_6$ in solid methane gives rise to new 1932 and 1886 cm^{-1} bands that shift to 1939 and 1894 cm^{-1} in solid argon and are assigned to $W(CO)_4$.[8] Our neon matrix bands at 1954.0 and 1909.0 cm^{-1} lead to the gas phase absorptions for $W(CO)_4$ at 1957 and 1909 cm^{-1}.[13] The consistency in observations for these $M(CO)_4$ species using three different experimental approaches provides strong support for the assignments.

M(CO)$_5$. The next strongest absorption with Mo and CO appeared at 1984.5 cm^{-1} in solid neon: a weaker 1944.6 cm^{-1} absorption increased with the 1984.5 cm^{-1} band on annealing (Figure 1), and both bands were stronger with 0.2% CO. Again, both bands showed carbonyl shifts with ^{12}CO and C^{18}O substitution, but no mixed isotopic components could be resolved. Photodissociation of $Mo(CO)_6$ in solid methane produced strong new 1967 and 1926 cm^{-1} bands that were conclusively identified as e and a_1 modes of $Mo(CO)_5$ on the basis of mixed ^{12}CO, ^{13}CO substitution.[8] These bands shifted to 1973 and 1933 cm^{-1} in solid argon.[8] The above neon matrix bands at 1984.5 and 1944.6 cm^{-1} approach transient gas phase observations[13] for $Mo(CO)_5$ at 1990 and 1942 cm^{-1}.

The next strongest absorption with W and CO in solid neon appeared at 1975.9 cm^{-1} and increased on annealing with a weaker 1941.1 cm^{-1} counterpart. In fact, after 10 K annealing, 1975.9 cm^{-1} is the strongest absorption present (Figure 5) as is the ^{13}CO counterpart at 1932.3 cm^{-1} (Figure 6). No intermediate component could be observed with mixed ^{12}CO + ^{13}CO because of the appearance of $W(^{13}CO)_6$ (Figure 7). Again, the neon matrix bands at 1975.6 and 1941.1 cm^{-1} fall in line with methane and argon matrix[8] bands at 1957, 1963 cm^{-1} and at 1926, 1932 cm^{-1} and transient gas phase[13] bands at 1980 and 1942 cm^{-1} and substantiate the formation of $W(CO)_5$ from W atoms and CO molecules in solid neon.

M(CO)$_6$. The culmination of group 6 metal atom reactions with successive CO molecules is the stable metal hexacarbonyl employed as a precursor in previous photodissociation investigations.[4−9,11−13,15,16] The saturated $Mo(CO)_6$ and $W(CO)_6$ molecules are observed on annealing in solid neon through strong t_2 absorptions measured within ±3 cm^{-1} of the gas phase values.[13,36]

MCO$^+$. In addition to being a softer matrix that allows more aggregation on diffusion, the neon matrix is often more effective for trapping molecular ions. The CO^+, $(CO)_2^+$, and $(CO)_2^-$ molecular ions[18,37] are observed in these experiments. Laser ablation produces a small proportion of cations and electrons in addition to metal atoms so cation carbonyls are potential products.[14,38]

The highest metal-dependent product fundamental absorption observed with Mo is a weak 2189.1, 2187.7 cm^{-1} doublet. This band increased on annealing to 6 (not shown) and 8 K, disappeared on full arc photolysis, reappeared on annealing to 10 K (not shown), and increased on final annealing to 12 K (Figure 2). An identical experiment with 10% as much CCl_4 as CO gave more than double the 2189.1, 2187.7 cm^{-1} bands on sample deposition and on annealing (Figure 2). The CCl_4 molecule is an effective electron trap, which favors the trapping

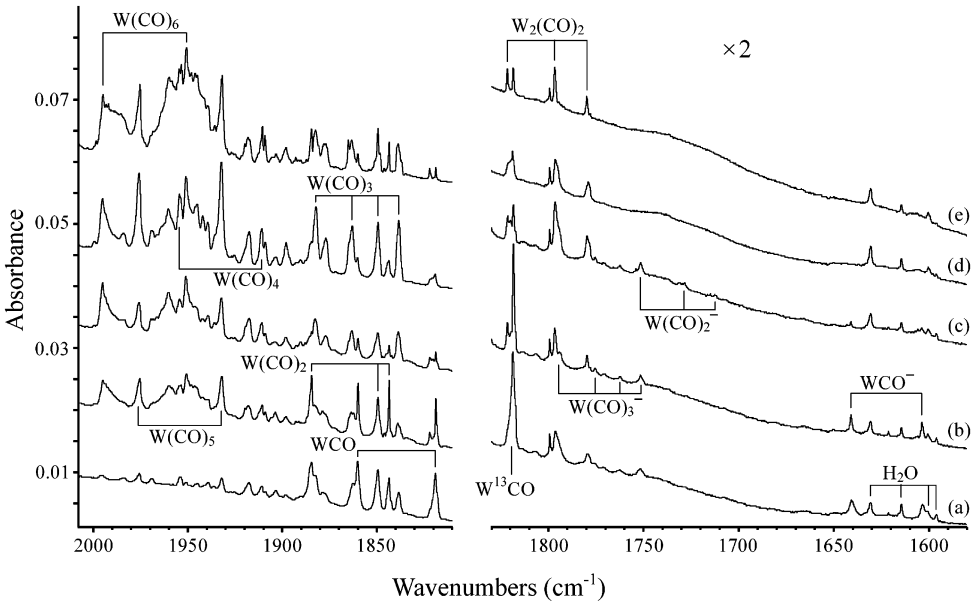

Figure 7. Infrared spectra in the 2008−1810 and 1830−1580 cm^{-1} regions for laser-ablated W codeposited with carbon monoxide in neon at 4 K. (a) 0.1% ^{12}CO + 0.1% ^{13}CO deposited for 30 min, (b) after annealing to 8 K, (c) after $\lambda > 470$ nm photolysis for 15 min, (d) after $\lambda > 290$ nm photolysis, and (e) after annealing to 10 K.

of cation species[14,38] and supports assignment of the above bands to $MoCO^+$ in solid neon.

The ^{13}CO counterparts shifted under unreacted ^{12}CO absorption in the sample. The ^{12}CO counterpart bands were again observed with mixed $^{12}CO + {}^{13}CO$, and the median region was free of an intermediate component, which provides evidence for the monocarbonyl cation. Fortunately, $C^{18}O$ substitution shifted these bands below ^{12}CO to 2137.3, 2135.9 cm^{-1}, which are appropriate for a carbonyl vibration. The $C^{18}O$ counterpart bands exhibited the same annealing and photolysis behavior illustrated in Figure 2 for the ^{12}CO counterparts. The 2189.1, 2187.7 cm^{-1} bands are assigned to the $MoCO^+$ cation in solid neon.

The highest metal-dependent product fundamental absorption observed with laser-ablated W and CO is at 2125.5 cm^{-1}. This weak absorption increased on 6 and 8 K annealing, photobleached with UV light, and reappeared in part on 10 K annealing, almost the same behavior as the above $MoCO^+$ bands. The 2125.5 cm^{-1} band was enhanced on doping with CCl_4 as expected for a cation absorption.[14,38] The ^{13}CO and $C^{18}O$ counterpart absorptions were observed at 2077.8 and 2076.5 cm^{-1}, respectively, and define a C−O vibration with increased C and decreased O participation relative to CO itself. The 2125.5 cm^{-1} band is assigned to WCO^+ in solid neon.

Our DFT calculations predict $^6\Sigma^+$ ground states for $MoCO^+$ and WCO^+, in agreement with previous ab initio work[39] on $MoCO^+$, with C−O frequencies at 2119.6 and 2077.6 cm^{-1}, respectively, which are 68 and 48 cm^{-1} below the observed values. Furthermore, we compute the C−O frequencies 248 (BP86) and 285 cm^{-1} (B3LYP) higher for $MoCO^+$ than for MoCO as compared to the 308 cm^{-1} experimental difference. This is very good agreement considering the approximate nature of the calculations. The frequencies are predicted 230 (BP86) and 265 cm^{-1} (B3LYP) higher for WCO^+ than for WCO, which are in better agreement with the 266 cm^{-1} neon matrix difference. Hence, our DFT calculations support the neon matrix observations of $MoCO^+$ and WCO^+.

$Mo(CO)_2^+$. The 2178.2 cm^{-1} absorption with Mo and CO in solid neon (Figure 2) exhibits similar growth on annealing and demise on photolysis as the $MoCO^+$ absorptions at 2189.1, 2187.7 cm^{-1}. Following the neon matrix observation[17] of $Cr(CO)_2^+$ absorption 22 cm^{-1} below $CrCO^+$, the 2178.2 cm^{-1} absorption is assigned to $Mo(CO)_2^+$. Both ^{13}CO and $C^{18}O$ counterpart absorptions were observed (Table 1), but the intermediate region was covered by ^{12}CO species.

Our BP86 calculations predict a $^4B_2$ ground state for $Mo(CO)_2^+$ with $^6\Sigma_g^+$ just 7.6 kcal/mol higher (Table 7). However, the strong $^6\Sigma_g^+$ state σ_u frequency predicted at 2139 cm^{-1} is much closer to the observed 2178.2 cm^{-1} value than the $^4B_2$ state b_2 mode prediction at 2020 cm^{-1}; furthermore, the corresponding higher frequency a_1 mode is not observed. Hence, we believe $Mo(CO)_2^+$ has the $^6\Sigma_g^+$ ground state like $Cr(CO)_2^+$,[17] which is in agreement with an ab initio investigation.[39] A similar B3LYP calculation finds the $^6\Sigma_g^+$ state lower by 1.2 kcal/mol (Table 8).

$M(CO)_n^-$. One band in Mo experiments clearly behaves as a molecular anion absorption. This band at 1718.7 cm^{-1} increases and sharpens on annealing to 8 K, decreases slightly on $\lambda > 470$ nm photolysis, decreases more on $\lambda > 380$ nm irradiation (not shown), disappears on $\lambda > 290$ nm photolysis, and barely reappears on 10 K annealing (Figure 1). The experiments shown in Figure 2 revealed 5% as much 1718.7 cm^{-1} absorption with CCl_4 added to the sample to trap ablated electrons as compared to the normal sample without CCl_4. Hence, extra electrons enhance the 1718.7 cm^{-1} absorption, and an electron capture product is indicated.[14,38]

The ^{13}CO and $C^{18}O$ shifts show slightly increased carbon and decreased oxygen participation in this normal mode. The mixed $^{12}CO + {}^{13}CO$ experiment reveals a sharp triplet absorption, which indicates the participation of two equivalent CO submolecules in this mode. The central component at 1696.4 cm^{-1} is 3.2 cm^{-1} below the median pure isotopic band, which shows that the out-of-phase $Mo(^{12}CO)(^{13}CO)^-$ stretching mode is interacting with an in-phase mode some 100 cm^{-1} higher, but this mode is too weak to be observed.

Our BP86 calculation predicts a $^2A_1$ ground state for $Mo(CO)_2^-$ with equally strong b_2 and a_1 fundamentals at 1698 and 1768 cm^{-1} and a $^4\Sigma_g^-$ state just 5.1 kcal/mol higher with very strong σ_u mode at 1722 cm^{-1}. The B3LYP functional finds

TABLE 7: Spectroscopic Constants of the Lowest States of $Mo(CO)_2^+$ and $W(CO)_2^+$ Calculated at the BP86/ LANL2DZ(Mo, W)+6-311+G*(C,O) Level

	$Mo(CO)_2^+$			$W(CO)_2^+$		
	$^2B_1$	$^4B_2$	$^6\Sigma_g^+$	$^2B_2$	$^4B_2$	$^6\Sigma_g^+$
r_e(M−C) (Å)	1.954	1.997	2.224	1.957	1.961	2.159
r_e(C−O)	1.153	1.148	1.134	1.153	1.152	1.136
<CMC (deg)	96.5	88.5	180.0	89.5	89.3	180.0
<MCO (deg)	179.3	179.9	180.0	179.9	179.9	180.0
$\omega(a_1)$, π_u	95(1)[a]	93(1)	13(1)	97(1)	98(0)	26(0)
$\omega(a_2)$, π_u	346(0)	319(0)	13(1)	349(0)	348(0)	26(0)
$\omega(b_1)$, π_g	345(3)	325(1)	259(0)	355(1)	351(0)	287(50)
$\omega(b_2)$, π_g	363(1)	357(2)	259(0)	390(0)	392(1)	292(0)
$\omega(b_2)$, σ_u	422(72)	423(17	285(27)	451(40)	462(26)	292(0)
$\omega(a_1)$, π_u	449(3)	439(1)	293(0)	478(3)	475(3)	353(0)
$\omega(a_1)$, σ_g	588(1)	574(1)	295(0)	576(0)	575(1)	372(2)
$\omega(b_2)$, σ_u	1960(1159)	2020(666)	2139(767)	1978(859)	1995(736)	2106(1069)
$\omega(a_1)$, σ_g	2034(211)	2077(194)	2174(0)	2048(221)	2054(220)	2160(0)
ΔE_{tot}[b] (eV)	+8.27	+7.73	+8.06	+8.29	+7.61	+8.16

[a] Frequencies, cm^{-1} (infrared intensities, km/mol). [b] Energy with respect to calculated $^3A_2$ ground states of neutral parents.

TABLE 8: Spectroscopic Constants for the $Mo(CO)_2$ Ions Calculated at the B3LYP/LANL2DZ(Mo) +6-311+G*(C,O) Levels

	$Mo(CO)_2^-$			$Mo(CO)_2^+$		
	$^2\Delta_g$	$^2A_2$	$^4\Sigma_g^-$[a]	$2A_2$[b]	$^4B_2$	$^6\Sigma_g^+$
r_e(Mo−C) (Å)	1.997	1.918	2.023	1.985	2.036	2.268
r_e(C−O)	1.171	1.177	1.179	1.135	1.131	1.119
<CMoC (deg)	180.0	76.4	180.0	82.1	89.3	180.0
<MoCO (deg)	180.0	177.7	180.0	179.3	179.8	180.0
$\omega(a_1)$, π_u	64(1)	102(0)	34(2)	101(1)	92(1)	33(1)
$\omega(a_2)$, π_u	64(1)	378(0)	34(2)	349(0)	318(0)	33(1)
$\omega(b_1)$, π_g	316(0)	396(18)	256(0)	364(1)	325(0)	257(0)
$\omega(b_2)$, π_g	316(0)	429(27)	256(0)	383(0)	352(2)	257(0)
$\omega(b_2)$, σ_u	431(135)	480(65)	423(66)	398(47)	387(22)	265(19)
$\omega(a_1)$, σ_g	447(0)	519(19)	427(0)	437(6)	402(2)	264(0)
$\omega(a_1)$,π_u	528(26)	638(5)	568(4)	588(3)	561(2)	296(0)
$\omega(b_2)$, σ_u	1840(3691)	1784(1425)	1782(4472)	2086(982)	2131(807)	2252(702)
$\omega(a_1)$, σ_g	1959(0)	1908(1890)	1911(0)	2152(366)	2185(260)	2278(0)
ΔE_{tot}[c] (eV)	−0.71	−1.06	−1.31	+7.78	+7.28	+7.23

[a] $^4B_1$ is a transition state; a $^6\Pi$ state is above by 0.81 eV. [b] $^2\Delta_g$ is higher by 0.77 eV. [c] With respect to the ground $^3A_2$ state of the neutral parents.

TABLE 9: Spectroscopic Consants of the Lowest States of $Mo(CO)_2^-$ and $W(CO)_2^-$ Calculated at the BP86, LANL2DZ(Mo, W)+6-311+G*(C,O) Level

	$Mo(CO)_2^-$			$W(CO)_2^-$		
	$^2A_1$[a]	$^4\Sigma_g^-$	$^4A_2$	$^2A_1$	$^2\Delta_g$	$^4B_1$[b]
r_e(M−C) (Å)	1.873	2.016	1.929	1.877	1. 986	1.997
r_e(C−O)	1.208	1.195	1.193	1.212	1. 194	1.200
<CMC (deg)	87.5	180.0	74.6	87.4	180.0	166.1
<MCO (deg)	179.9	180.0	179.7	179.3	180.0	173.3
$\omega(a_1)$, π_u[c]	93(1)	17(2)	95(0)	92(1)	40(2)	33(4)
$\omega(a_2)$, π_u	373(0)	17(2)	356(0)	290 (0)	40(2)	289(0)
$\omega(b_1)$, π_g	385(12)	263(0)	350(61)	387(8)	325(0)	573(1)
$\omega(b_2)$, π_g	411(5)	263(0)	366(355)	430(3)	325(0)	274(4)
$\omega(b_2)$, σ_u	542(3)	429(40)	434(94)	545(1)	432(32)	432(13)
$\omega(a_1)$, σ_g	542(0)	430(0)	513(3.9)	549(1)	470(0)	465(0)
$\omega(a_1)$, π_u	656(2)	555(5)	591(44)	608(10)	589(1)	584(1)
$\omega(b_2)$, σ_u	1698(1266)	1722(3363)	1708(2395)	1698(1365)	1740(3125)	1706(3106)
$\omega(a_1)$, σ_g	1768(1292)	1837(0)	1843(851)	1763(1109)	1856(0)	1822(68)
ΔE_{tot}[d] (eV)	−1.67	−1.45	−1.05	−1.94	−1.63	−1.66

[a] $^2\Delta_g$ is a transition state. [b] $^4A_2$ is above by 0.12 eV. [c] Frequency, cm^{-1} (infrared intensity, km/mol). [d] With respect to the computed $^3A_2$ ground states of the neutral parents. Sextet states of both anions are above their ground $^2A_1$ states by ≈1.30 eV.

the $^4\Sigma_g^+$ ground state (Table 8). Clearly, the $^4\Sigma_g^-$ state fits our spectrum much better.

Weak 1771.4 and 1699.6 cm^{-1} absorptions in the Mo system could also be due to anions, as these bands are eliminated by CCl_4 doping, but there is less compelling evidence. Both bands sharpen on annealing and decrease on photolysis like the $Mo(CO)_2^-$ absorption. If the W system is taken as an example, the 1699.6 and 1771.4 cm^{-1} bands are good candidates for $MoCO^-$ and $Mo(CO)_3^-$, respectively. Our BP86 calculations predict the $^4\Sigma^-$ ground state for $MoCO^-$ and a 1633.2 cm^{-1} frequency, which is too low for the above assignment. However, the 5.5 kcal/mol higher $^4\Pi$ state has a 1759.0 cm^{-1} frequency prediction. If the 1699.0 cm^{-1} absorption is due to $MoCO^-$, a $^4\Pi$ ground state is likely.

The W system reveals three bands in the anion region. These bands at 1640.8, 1751.5, and 1794.2 cm^{-1} increase slightly on

TABLE 10: Comparison of Gas Phase Neon and Argon Matrix Frequencies (cm^{-1}) for Group 6 Carbonyls

	Cr				Mo			W		
	gas[a]	Ne[b]	Ar[b]	Ar[c]	gas[a]	Ne[d]	Ar	gas[a]	Ne[d]	Ar
M(CO)		2018.4	1975.6			1881.2	1862.6[e]		1859.9	1848.8[e]
$M(CO)_2$		1982.1	1970.8							
		1832.9	1821.5			1895.2	1891.9[e]		1884.5	
$M(CO)_3$	1880	1873.8	1864.5	1867	1891	1886.1	1869[c]		1882.4	1865[c]
			680.8							
			483							
$M(CO)_4$		2066.1	2058.5							
	1957	1952.2	1938.7	1940	1972	1965.7	1951[c]	1957	1954.0	1939[c]
			1933.3	1934						
	1920	1911.2	1895.3	1896	1911	1908.9	1895[c]	1909	1909.0	1894[c]
			433.3							
$M(CO)_5$	1980	1976.2	1965.4	1966	1990	1984.5	1973[c]	1980	1975.9	1963[c]
	1948			1936	1942	1944.6	1933[c]	1942	1941.1	1932[c]
			603.1							
			453.7							
$M(CO)_6$	2000	1998.8	1990	1990	2003	2000.6	1992[c]	1998	1995.3	1986[c]
	668	672.6	670	596	598.6		587	588.5		

[a] Refs 11−16; Table 3 of ref 13a. [b] Ref 17. [c] Table 4 of ref 8a. [d] This work, 4 K. [e] Ref 23.

annealing to 8 K (Figure 5), but $\lambda > 470$ nm photolysis decreases the strongest of these at 1640.8 cm^{-1} while markedly increasing the 1751.5 cm^{-1} feature, slightly increasing the 1794.2 cm^{-1} band, and decreasing the WCO and $W(CO)_2$ absorptions. Irradiation at $\lambda > 380$ nm (not shown) virtually completes the demise of the 1640.8 cm^{-1} band and slightly decreases the others, and $\lambda > 290$ nm irradiation removes all three absorptions and the WCO^+ band. Subsequent annealing restores only a part of the WCO^+ absorption. The above bands are reduced markedly on doping with CCl_4 to trap electrons.

These bands exhibit ^{13}CO and $C^{18}O$ shifts with increased carbon and decreased oxygen participation in this mode relative to CO indicating coupling of carbon with another atom. Of more importance, the mixed $^{12}CO + {}^{13}CO$ experiment reveals a doublet for the strongest 1640.8−1603.3 cm^{-1} bands that identifies the vibration of a single CO subunit. After $\lambda > 470$ nm photolysis, the 1751.5 cm^{-1} band gives a triplet profile with one intermediate component at 1728.4 cm^{-1}, which denotes the vibration of two equivalent CO groups. The intermediate mixed isotopic band is 3.4 cm^{-1} below the median of the pure isotopic 1751.5−1712.2 cm^{-1} bands as expected for the b_2 mode of a dicarbonyl with the a_1 mode some 100 cm^{-1} higher. The 1794.2 band shows a quartet profile with weaker intermediate bands at 1775.7 and 1762.6 cm^{-1}, like $W(CO)_3$, which is characteristic of the doubly degenerate mode in a trigonal species.[14,35] Hence, the anion bands at 1640.8, 1751.5, and 1794.2 cm^{-1} can be assigned, respectively, to the $W(CO)_{1,2,3}^-$ anions.

Some qualitative photodetachment information is found in our photolysis experiment. The WCO^- anion detaches with $\lambda > 470$ nm light whereas $W(CO)_2^-$ and $W(CO)_3^-$ do not; however, $\lambda > 380$ nm irradiation starts to remove the latter absorptions. This is more energy than the gas phase photodetachment threshold for $W(CO)_3^-$, namely, 1.86 eV (666 nm),[40] which is typical for matrix-isolated molecular anions.[14] Here, using a mercury arc, we probably need a dissociative electronic transition.

Although only approximate, our BP86 calculations predict low $^2\Delta$, $^4\Pi$, and $^4\Sigma^-$ states for WCO^-, but it is unlikely that $^2\Delta$ can be formed by electron capture of WCO ($^5\Pi$) or dissociative capture of a quintet $W(CO)_2$ state. The calculation finds a $^4\Pi$ state for WCO^- with 1730 cm^{-1} C−O frequency and a $^4\Sigma^-$ state just 6.9 kcal/mol higher with 1623.4 cm^{-1} C−O frequency. Furthermore, these states have short W−C bonds and exhibit more W−C, C−O vibrational interaction as found in $^{12}CO/^{13}CO$ and $C^{16}O/C^{18}O$ isotopic frequency ratios ($^4\Sigma^-$ predicted 1.0265, 1.0195) and ($^4\Pi$ predicted 1.0253, 1.0209 ratios, respectively). The observed 1640.8 cm^{-1} WCO^- fundamental fits the $^4\Sigma^-$ state prediction better and suggests that $^4\Sigma^-$ is the ground state of WCO^-.

Our BP86 calculations do not give a clear means of identifying the ground state of $W(CO)_2^-$. The BP86 functional predicts a $^2A_1$ ground state and strong 1698 cm^{-1} b_2 frequency, which is below the 1751.5 cm^{-1} neon matrix observation and an unlikely electron capture product for $^5A_2$ $W(CO)_2$ (Table 9). The $^4B_1$ $W(CO)_2^-$ state is only 6.4 kcal/mol higher, but the frequency is still too low. B3LYP calculations narrow the doublet−quartet energy separation, and we believe that the anion ground state is probably a quartet.

$M_2(CO)_2$. Absorptions at 1797.7 cm^{-1} with Mo and 1821.8 cm^{-1} with W increase slightly on annealing and photolysis (Figures 1 and 5). These bands show ^{13}CO and $C^{18}O$ shifts expected for C−O vibrations. Of more importance, the mixed $^{12}CO + {}^{13}CO$ experiments show sharp triplet absorptions with stronger intermediate components that indicate the vibration of two equivalent CO subunits. The intermediate bands for Mo (1775.3 cm^{-1}) and W (1796.8 cm^{-1}) are 2.8 and 4.0 cm^{-1} below the mean of pure isotopic bands, which again points to a higher unobserved symmetric C−O stretching mode relative to the observed antisymmetric stretching mode. These bands are somewhat higher than the very strong 1735.4 cm^{-1} absorption observed for $Cr_2(CO)_2$ in the corresponding chromium experiments.[17] Extensive DFT calculations suggest that $Cr_2(CO)_2$ is a planar species ($^3A_2$ state) with two equivalent CO and two slightly nonequivalent Cr atoms.

Reaction Mechanisms. As found for Cr atoms,[10,17] Mo and W atoms react with CO on codeposition with excess neon and on annealing the solid to form all of the mononuclear carbonyls $M(CO)_n$ ($n = 1-6$). Whereas a relatively large yield of CrCO ($^7A'$) and small yield of $Cr(CO)_2$ ($^5A_1$) were obtained,[17] we find the reverse with Mo and intermediate behavior, namely, moderate yields of both with W. The ground states of Mo and W are $^7S_3$ and $^5D_0$, respectively.[41] Reaction 1a appears to be less favorable than reaction 1b in these experiments, which may be due to the lack of spin conservation. Once formed, the MCO species readily add CO to produce the dicarbonyls, reaction 2. The yield of $M(CO)_3$ is small implying a slow reaction 3, but once formed, $M(CO)_3$ reacts rapidly with CO to form $M(CO)_{4,5,6}$ as found in the gas phase investigations.[11−13,15,16] Because the

saturated $M(CO)_6$ complexes have singlet ground states, fast reaction 4 suggests singlet states for the unsaturated $M(CO)_{3,4,5}$ intermediates.

$$Mo\ (^7S_3) + CO\ (^1\Sigma^+) \rightarrow MoCO\ (^5\Pi) \quad (1a)$$

$$W\ (^5D_0) + CO\ (^1\Sigma^+) \rightarrow WCO\ (^5\Pi) \quad (1b)$$

$$MCO\ (^5\Pi) + CO\ (^1\Sigma^+) \rightarrow M(CO)_2\ (^5A_2) \quad (2)$$

$$M(CO)_2\ (^5A_2) + CO\ (^1\Sigma^+) \rightarrow M(CO)_3\ (\text{singlet}) \quad (3)$$

$$M(CO)_3\ (\text{singlet}) + 1,2,3CO\ (^1\Sigma^+) \rightarrow M(CO)_{4,5,6}\ (\text{singlet}) \quad (4)$$

The metal cations produced on laser ablation also react with CO to form the MCO^+ cation carbonyls.[14,38] Electrons from the ablation process are captured by the unsaturated carbonyl fragments to form metal carbonyl anions. The role of added CCl_4 is to capture ablated electrons and thus prevent the formation of carbonyl anions and allow the survival of more MCO^+ reaction product.[14,38] We cannot rule out dissociative capture processes such as reaction 6b.

$$Mo^+\ (^6S) + CO\ (^1\Sigma^+) \rightarrow MoCO^+\ (^6\Sigma^+) \quad (5a)$$

$$W^+\ (^6D) + CO\ (^1\Sigma^+) \rightarrow WCO^+\ (^6\Sigma^+) \quad (5b)$$

$$M(CO)_2\ (^5A_2) + e^- \rightarrow M(CO)_2^-\ (\text{quartet}) \quad (6a)$$

$$M(CO)_2\ (^5A_2) + e^- \rightarrow MCO^-\ (\text{quartet}) + CO \quad (6b)$$

Conclusions

Laser-ablated Mo and W atoms react with CO in excess neon to produce the same unsaturated $M(CO)_{3,4,5}$ species produced from photodissociation of $M(CO)_6$, based on comparison of gas phase, neon matrix, and argon matrix frequencies (Table 10). The neon matrix frequencies ($^{12}C^{16}O$, $^{13}C^{16}O$, $^{12}C^{18}O$) are between argon matrix and gas phase values. In addition, laser ablation produces cations and electrons, which react to form the $M(CO)_{1,2}^+$ cations and $M(CO)_{1,2,3}^-$ anions as identified from neon matrix infrared spectra.

Density functional calculations are useful for predicting ground states and vibrational frequencies of unsaturated transition metal carbonyls.[14,38] However, the Mo and W cases are pushing the DFT and pseudopotential approximations to the limit. Hence, we rely on experimental matrix frequencies to select the ground state from calculated frequencies rather than from calculated energies.

Acknowledgment. We gratefully acknowledge support for this work from N.S.F. Grants CHE97-00116 and CHE00-78836 and N.A.S.A. Grant NCC 2-5415 and helpful discussions with C. W. Bauschlicher, Jr. and R. N. Perutz.

References and Notes

(1) Cotton, F. A.; Wilkinson, G.; Murillo, C. A.; Bochmann, M. *Advanced Inorganic Chemistry*, 6th ed.; Wiley: New York, 1999.

(2) Collman, J. P.; Hegedus, L. S.; Norton, J. R.; Fink, R. G. *Principles and Applications of Organotransition Metal Chemistry*; University Science Books: Mill Valley, CA, 1987.

(3) Hoffmann, R. *Angew. Chem., Intl. Ed. Engl.* **1982**, *21*, 711.

(4) Graham, M. A.; Poliakoff, M.; Turner, J. J. *J. Chem. Soc. A* **1971**, 2939.

(5) Kundig, E. P.; Ozin, G. A. *J. Am. Chem. Soc.* **1974**, *96*, 3820.

(6) Perutz, R. N.; Turner, J. J. *Inorg. Chem.* **1975**, *14*, 262.

(7) Perutz, R. N.; Turner, J. J. *J. Am. Chem. Soc.* **1975**, *97*, 4791.

(8) (a) Perutz, R. N.; Turner, J. J. *J. Am. Chem. Soc.* **1975**, *97*, 4800. (b) Perutz, R. N., Ph.D. Thesis, University of Cambridge, 1974.

(9) Burdett, J. K.; Graham, M. A.; Perutz, R. N.; Poliakoff, M.; Rest, A. J.; Turner, J. J.; Turner, R. F. *J. Am. Chem. Soc.* **1975**, *97*, 4805.

(10) Bach, S. B. H.; Taylor, C. A.; Van Zee, R. J.; Vala, M. T.; Weltner, W., Jr. *J. Am. Chem. Soc.* **1986**, *108*, 7104.

(11) (a) Seder, T. A.; Church, S. P.; Weitz, E. *J. Am. Chem. Soc.* **1986**, *108*, 4721. (b) Weitz, E. *J. Phys. Chem.* **1987**, *91*, 3945; **1994**, *98*, 11256.

(12) Fletcher, T. R.; Rosenfeld, R. N. *J. Am. Chem. Soc.* **1985**, *107*, 2203.

(13) (a) Ishikawa, Y.; Brown, C. E.; Hackett, P. A.; Rayner, D. M. *J. Phys. Chem.* **1990**, *94*, 2404. (b) Rayner, D. M.; Ishikawa, Y.; Brown, C. E.; Hackett, P. A. *J. Chem. Phys.* **1991**, *94*, 5471. (b) Rayner, D. M.; Ishikawa, Y.; Brown, C. E.; Hackett, P. A. *J. Chem. Phys.* **1991**, *94*, 5471.

(14) Zhou, M. F.; Andrews, L.; Bauschlicher, C. W., Jr. *Chem. Rev.* **2001**, *101*, 1931.

(15) Ganske, J. A.; Rosenfeld, R. N. *J. Phys. Chem.* **1989**, *93*, 1959 (Mo).

(16) Ishikawa, Y.; Hackett, P. A.; Rayner, D. M. *J. Phys. Chem.* **1988**, *92*, 3863 (W).

(17) Andrews, L.; Zhou, M. F.; Gutsev, G. L.; Wang, X. *J. Phys. Chem. A* **2003**, *107*, 561.

(18) Jacox, M. E. *Chem. Phys.* **1994**, *189*, 149.

(19) (a) Fournier, R. *J. Chem. Phys.* **1993**, *98*, 8041. (b) Fournier, R. *J. Chem. Phys.* **1993**, *99*, 1801.

(20) Adamo, C.; Lelj, F. *J. Chem. Phys.* **1995**, *103*, 10605; *Chem. Phys. Lett.* **1995**, *246*, 463.

(21) Gutsev, G. L.; Andrews, L.; Bauschlicher, C. W., Jr. To be published.

(22) Tan, H.; Liao, M.; Dai, D.; Balasubramanian, K. *J. Phys. Chem. A* **1998**, *102*, 6801.

(23) Souter, P. F.; Andrews, L. *J. Am. Chem. Soc.* **1995**, *117*, 7350 (M + CO_2, CO).

(24) Burkholder, T. R.; Andrews, L. *J. Chem. Phys.* **1991**, *95*, 8697.

(25) Hassanzadeh, P.; Andrews, L. *J. Phys. Chem.* **1992**, *96*, 9177.

(26) Zhou, M. F.; Andrews, L. *J. Chem. Phys.* **1999**, *111*, 4230.

(27) Frisch, M. J.; Trucks, G. W.; Schlegel, H. B.; Scuseria, G. E.; Robb, M. A.; Cheeseman, J. R.; Zakrzewski, V. G.; Montgomery, J. A., Jr.; Stratmann, R. E.; Burant, J. C.; Dapprich, S.; Millam, J. M.; Daniels, A. D.; Kudin, K. N.; Strain, M. C.; Farkas, O.; Tomasi, J.; Barone, V.; Cossi, M.; Cammi, R.; Mennucci, B.; Pomelli, C.; Adamo, C.; Clifford, S.; Ochterski, J.; Petersson, G. A.; Ayala, P. Y.; Cui, Q.; Morokuma, K.; Malick, D. K.; Rabuck, A. D.; Raghavachari, K.; Foresman, J. B.; Cioslowski, J.; Ortiz, J. V.; Stefanov, B. B.; Liu, G.; Liashenko, A.; Piskorz, P.; Komaromi, I.; Gomperts, R.; Martin, R. L.; Fox, D. J.; Keith, T.; Al-Laham, M. A.; Peng, C. Y.; Nanayakkara, A.; Gonzalez, C.; Challacombe, M.; Gill, P. M. W.; Johnson, B. G.; Chen, W.; Wong, M. W.; Andres, J. L.; Head-Gordon, M.; Replogle, E. S.; Pople, J. A. *Gaussian 98*, revision A.6; Gaussian, Inc.: Pittsburgh, PA, 1998.

(28) (a) Becke, A. D. *Phys. Rev. A* **1988**, *38*, 3098. (b) Perdew, J. P. *Phys. Rev. B* **1983**, *33*, 8822. (c) Perdew, J. P.; Wang, Y. *Phys. Rev. B* **1992**, *45*, 13244.

(29) (a) Becke, A. D. *J. Chem. Phys.* **1993**, *98*, 5648. (b) Stevens, P. J.; Devlin, F. J.; Chablowski, C. F.; Frisch, M. J. *J. Phys. Chem.* **1994**, *98*, 11623.

(30) (a) McLean, A. D.; Chandler, G. S. *J. Chem. Phys.* **1980**, *72*, 5639. (b) Raghavachari, K.; Trucks, G. W. *J. Chem. Phys.* **1989**, *91*, 1062.

(31) (a) Hay, P. J.; Wadt, W. R. *J. Chem. Phys.* **1985**, *82*, 270. (b) Wadt, W. R.; Hay, P. J. *J. Chem. Phys.* **1985**, *82*, 284. (c) Hay, P. J.; Wadt, W. R. *J. Chem. Phys.* **1985**, *82*, 299.

(32) Calculations were also done for WCO^- using the SDD ECP. The state separations were similar, the bond lengths were within ±0.01 Å, and the frequencies were within 10 cm^{-1}.

(33) Manceron, L.; Alikhani, M. E. *Chem. Phys.* **1999**, *244*, 215.

(34) Andrews, L.; Zhou, M. F. *J. Phys. Chem. A* **1999**, *103*, 4167.

(35) Darling, J. H.; Ogden, J. S. *J. Chem. Soc., Dalton Trans.* **1972**, 2496.

(36) Jones, L. H.; McDowell, R. S.; Goldblatt, M. *Inorg. Chem.* **1969**, *8*, 2349.

(37) Thompson, W. E.; Jacox, M. E. *J. Chem. Phys.* **1991**, *95*, 735.

(38) Liang, B.; Zhou, M. F.; Andrews, L. *J. Phys. Chem. A* **2000**, *104*, 3905.

(39) Barnes, L. A.; Rosi, M.; Bauschlicher, C. W., Jr. *J. Chem. Phys.* **1990**, *93*, 609.

(40) Bengali, A. A.; Casey, S. M.; Cheng, C. L.; Dick, J. P.; Fenn, P. T.; Villalta, P. W.; Leopold, D. G. *J. Am. Chem. Soc.* **1992**, *114*, 5257.

(41) Moore, C. E. *Atomic Energy Levels, Vol. II*; National Bureau of Standards: United States, 1952.